A Modified Johnson–Cook Constitutive Model for the Compressive Flow Behaviors of the SnSbCu Alloy at High Strain Rates

Hanzhang Xu, Bin Zhao, Xiqun Lu, Zhigang Liu, Tongyang Li, Ning Zhong, and Xunshuai Yin

The SnSbCu alloy is widely used as the material for the main bearing in low-speed marine engines, and an accurate constitutive model is the foundation for studying the frictional behaviors of bearings. In this work, the compressive flow behaviors of the SnSbCu alloy were considered under the different strain rates (1000-5000 s^{-1}) and temperatures (20-110 °C) by quasi-static and split-Hopkinson pressure bar dynamic compression tests. First, the original Johnson–Cook model was used to describe the constitutive relation of the SnSbCu alloy at high strain rates, and the results predicted by the original model showed relatively large errors compared with the experimental results since the coupled effect of temperature and strain rate was omitted. Then, a modified Johnson–Cook constitutive model was developed to describe the compressive flow behaviors of the SnSbCu alloy, and the results predicted by this modified model agreed well with the experimental data. Moreover, a finite element analysis was also conducted to verify the accuracy of the modified Johnson–Cook model.

1. Introduction

The main bearing is one of the key components of a marine engine, and the tribological properties of this bearing have an important influence on the engine reliability and fuel economy. The material properties of the bearing coating play a crucial role in the lubrication performance, especially during the start–stop phase. Currently, material properties are often assumed to be constant in most studies. However, material properties are closely related to temperature and strain rate, and the working temperature of the coating material changes as the operating conditions change and the working strain rate sharply increases when contact occurs. Moreover, the surface contact can also produce heat, thereby increasing the temperature. Thus, tribological performance and material behavior interact with each other through temperature and strain rate. To investigate these properties of the main bearing, an accurate constitutive relation for the compressive flow behaviors of the bearing material should be revealed first. For low-speed marine engine, which is the focus of this work, the SnSbCu alloy is widely used as the main bearing material due to its good compliance, embeddedness and anti-seizure properties. Therefore, the constitutive

model of the SnSbCu alloy is studied in this work. Many works studying the mechanical properties of alloy materials have shown that the flow behaviors change obviously under different strain rates and temperatures (Ref 1-5). Under severe working conditions, especially the start and stop phases of the engine, the main bearing is in the stage of mixed lubrication, which means that more rigid peaks on the rough journal surface would penetrate into the softer bearing surface, similar to the grinding process, leading to high strain rates and temperature in the contact zone. The preliminary experiments conducted by the authors also indicated that the stress–strain curves of the SnSbCu alloy changed notably under different strain rates and temperatures. Therefore, it would be necessary to reveal the compressive flow behaviors and develop a relatively accurate constitutive model for the SnSbCu alloy material at high strain rates and temperatures considering its working conditions.

In the past few decades, many constitutive models have been proposed for alloy materials (Ref 6–8). Usually, there are three kinds of models to describe the constitutive relation: physical-based (Ref 9, 10), phenomenological-based (Ref 11-14) and empirical-based (Ref 15-18) models. All of these models include some material constants, which could be obtained by fitting the experimental results. Physical- and phenomenological-based models are more accurate than empirical-based models since the former are acquired based on physical assumptions. However, there are numerous material constants from precisely controlled experimental results. In contrast, the empirical model includes few material constants, which could be more easily obtained by some limited experiments; moreover, the empirical results have acceptable accuracy. Thus, the empirical model was preferred due to its higher practicability, especially when the constitutive model was integrated into the further investigations.

The Johnson–Cook (J–C) constitutive model (Ref 19-21) is one of the most widely used empirical models describing the flow behaviors of alloy materials due to its simple form. This model considers the strain rate hardening and thermal softening

Hanzhang Xu, Bin Zhao, Xiqun Lu, Zhigang Liu, and **Tongyang Li**, College of Power and Energy Engineering, Harbin Engineering University, Harbin 150001, China; **Ning Zhong**, Chongqing Hongjiang Machinery Co., Ltd, Chongqing 400000, China; and **Xunshuai Yin**, Shandong Institute of Space Electronic Technology, Yantai 264670, China. Contact e-mail: donglizhaobin@hrbeu.edu.cn.

effects. Aviral Shrot et al. (Ref 22) proposed a method for inversing the J–C model based on the Levenberg–Marquardt search algorithm and studied the cutting conditions using the original J–C model. Deng et al. (Ref 23) revealed the original J–C model for Gr2 titanium and studied its dynamic mechanical behavior. However, for the J–C model the three factors (strain, strain rate and temperature) are considered to be independent of each other, which is not sufficiently precise for some specific materials, as revealed by Samantary et al. (Ref 24) and He et al. (Ref 25). Therefore, many researchers have proposed various modifications on the basis of J–C model. For example, Li et al. (Ref 26) found that the original J–C model cannot fully describe the flow behaviors of T24 at high temperatures. To explain this phenomenon, they considered the influence of strain rate on the temperature softening effect to modify the strain hardening term and the temperature softening term of the J–C model. Wang et al. (Ref 27) discovered that the strain rate effect depended on the temperature and that the strain rate hardening and strain rate softening effects existed in the flow behaviors of Inconel 718, which was different from the original J–C model. Therefore, the model was modified by considering that the strain rate effect changed with respect to the strain rate and the temperature. Different researchers (Ref 28–33) also modified the original J–C constitutive model to meet the accuracy requirements for describing the flow behaviors of specific materials. However, to the author's knowledge, studies in the literature pertaining to the compressive flow behaviors of the SnSbCu alloy at high strain rates and high temperatures are still insufficient.

The constitutive model of a material is based on experimental data. The split-Hopkinson pressure bar (SHPB) (Ref 34, 35) is one of the most important experimental devices to measure the flow behaviors at high strain rates and high temperatures. An SHPB consists of a power system, a striker bar, an incident bar, a transmitted bar, an absorption bar, a dashpot and a measurement recording system. The striker bar impacts the incident bar at a certain speed, and a compressive stress wave is generated in the incident bar, which deforms the incident bar and transmitted bar. The compressive stress wave is reflected and transmitted at the front and back interfaces of the specimen, and the strain pulses are recorded by the strain gauge attached to the incident bar and the transmitted bar, so that the dynamic stress–strain relationship of the specimen can be calculated. Due to its high precision, SHPB test has been widely used in the field of material testing.

The purpose of this study is to describe the flow behaviors of the SnSbCu alloy at high strain rates (1000-5000 s^{-1}) in the temperature range of 20 °C to 110 °C using the modified Johnson–Cook constitutive model, which considers the influence of temperature on the strain rate effect. The SHPB tests and quasi-static compressive experiments were used to obtain the modified model, and a finite element simulation was employed to demonstrate the effectiveness of this model.

2. Materials and Experimental Procedures

2.1 Materials

Differential scanning calorimeter (DSC) was used to investigate the changes in the heat absorption rate and heat release rate in the SnSbCu alloy as the temperature increased from 0 to 110 °C to determine whether this material underwent a phase change within this temperature range. If there are phase transitions, there would be peaks and vice versa. As Fig. 1 shows, the heat flux of this alloy material is smooth, and no heat flux peak exists, which means there is no phase change in the temperature range of 0-110 °C.

The Vickers hardness of the material was measured (see Table 1) with an HTV-PHS30 testing system at temperatures of 60 °C, 90 °C and 120 °C. In this experiment, the pressure was held for 5 s after reaching the preset value. The heating rate was 6 °C/min, and the loading speed was 1 kg/15 s. Each measurement was conducted 5 times at the same temperature, and the average value was taken as the hardness at the specific temperature.

2.2 Experimental Procedure

An SHPB was used to measure the dynamic impact at temperatures of 20-110 °C and strain rates of 1000-5000 s^{-1}. The structural schematic diagram and a picture of the actual test setup for the SHPB are shown in Fig. 2. Cylindrical specimens that were 5 mm in height and 5 mm in diameter were prepared for the compression tests.

The incident wave, transmitted wave and reflected wave in the SHPB tests at a temperature of 20 °C and a strain rate of 2500 s^{-1} are shown in Fig. 3. As shown in Fig. 3, the incident wave, transmitted wave and reflected wave are smooth and stable, which indicates that the signal recording system and the experimental device are stable.

During the tests, the temperature should be controlled to ensure that the material temperature was stable. Figure 4 shows the heating process used to heat the specimens to the test temperature at a rate of 50 °C/min, and then, the test temperature was held for 15 min to ensure that the specimen temperature was uniform. After the tests, the specimen was air-cooled. Each experiment at each temperature and strain rate was carried out at least three times for the accuracy.

An Instron 5985 material universal testing machine was used to measure the quasi-static stress–strain curve of the alloy at the strain rate of 0.001 s^{-1} under different temperatures (20-110 °C). Cylindrical specimens that were 9 mm in height and 6 mm in diameter were prepared for the quasi-static tests.

In addition, to study the change of microscopic structure of SnSbCu alloy under different loading conditions, the com-
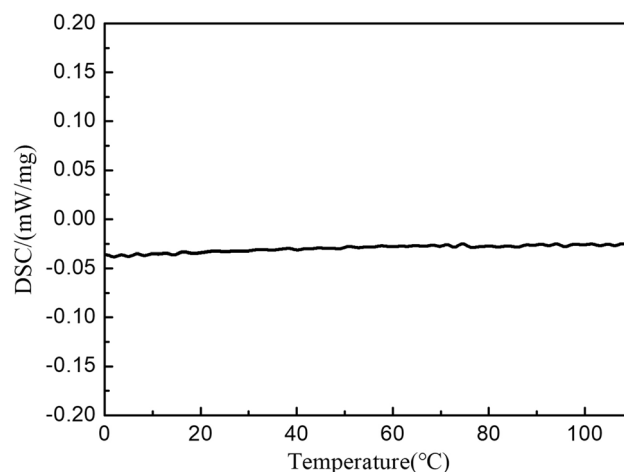

Fig. 1 DSC results of SnSbCu alloy

Table 1 The Vickers hardness of the SnSbCu alloy

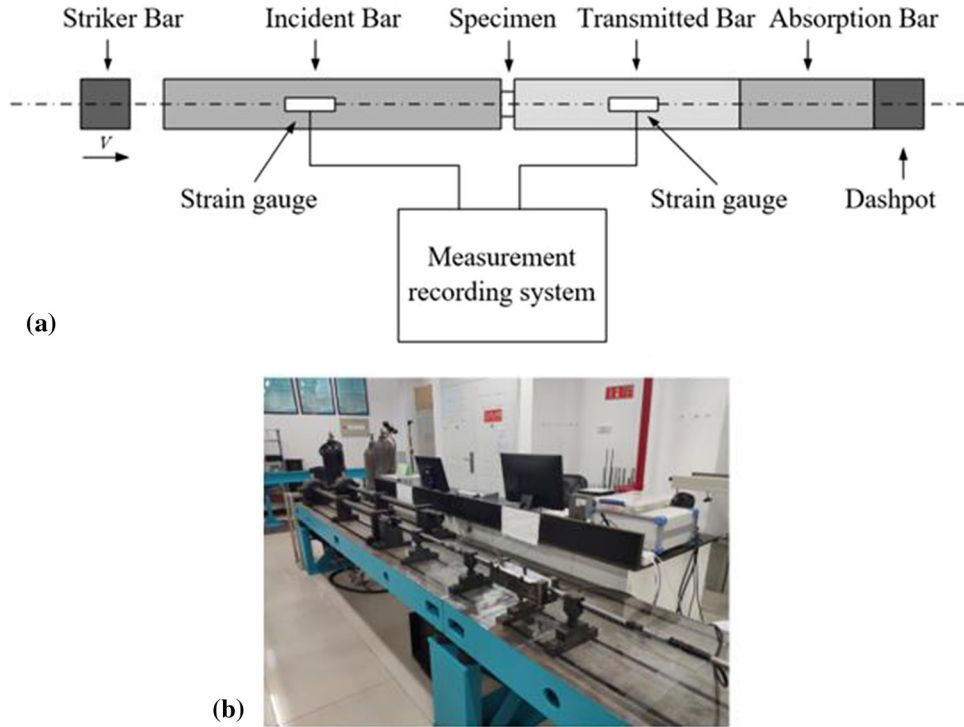| Temperature, °C	Vickers hardness, HV					Average value, HV
60	29.60	29.23	29.91	28.95	29.34	29.41
90	25.72	24.61	25.11	26.13	25.01	25.32
120	19.52	20.88	19.57	19.31	19.83	19.82

Fig. 2 Experimental equipment schematic of the SHPB: (a) structural schematic diagram and (b) actual test setup

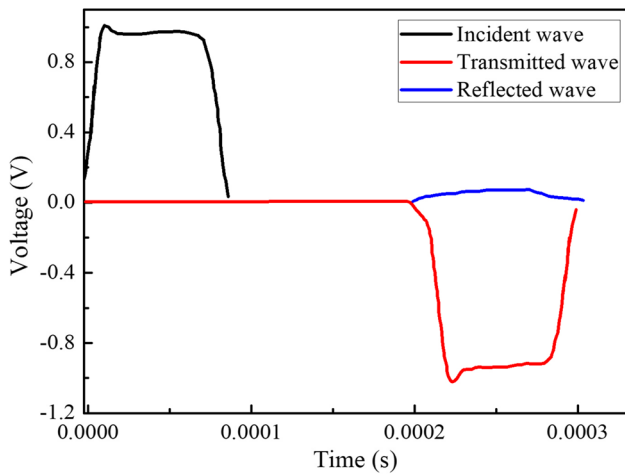**Fig. 3** Incident wave, transmitted wave and reflected wave in the SHPB tests at a temperature of 20 °C and a strain rate of 2500 s^{-1}

Fig. 4 Schematic diagram of the heating process

pressed specimens were used for scanning electron microscopy (SEM-Hitachi SU5000). The specimens were subsequently grounded wi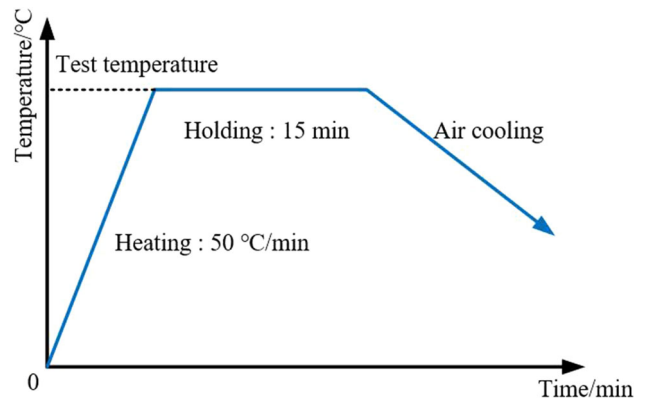th 400#, 800# and 2000# sandpaper with water, respectively. And then, the surfaces were polished with a polishing machine at 900 r/min. Surfaces of specimens were cleaned with distilled water and etched with 4 wt.% solution of nitric acid and alcohol for 20 s at room temperature. Finally, the specimens were dried by a blower.

3. Results and Discussion

3.1 Experimental Results

The true stress–strain curves under different strain rates (1000-5000 s^{-1}) and temperatures (20-110 °C) are obtained from the SHPB tests. Some selected results at three preset strain rates, 2500 s^{-1}, 4000 s^{-1} and 5000 s^{-1}, and four temperatures, 20 °C, 50 °C, 80 °C and 110 °C, are shown in Fig. 5. It should be noted that the true strain rates measured by the sensors in the test bench are slightly different from the preset values due to the dynamic effects of the SHPB. Figure 5 reveals that the true stress increases quickly as the true strain increases at the very beginning of testing, and then, the rate of increase notably decreases when the strain reaches a certain range corresponding to the initiation of yielding. Afterward, the true stress tends to gradually change. All curves at different temperatures and strain rates exhibit similar trends. In addition, it can be seen that the stress increases decreasing temperature at the same strain and strain rate.

Figure 6 shows the representative results of microstructure of the SnSbCu alloy obtained from scanning electron microscope (SEM) under different deformation conditions. It is obvious that the microstructures are closely related to strain rate and temperature. The result (Fig. 6a) shows regular distribution of phases in the matrix. The hard phases are quadrilateral, and the side length is about 200 μm. Figure 6(b)–(d) represents the change of microstructure at 20 °C as the strain rate increases

from 2500 to 5000 s^{-1}. Hard phases on the matrix are dispersed at low strain rate and more aggregate at high strain rate tending to quadrilateral. The influence of the temperature on the microstructure is shown in Fig. 6(b) and (e)–(g). It reveals that at low temperature, the distribution area of hard phase is smaller than that at high temperature. With the increase in temperature, the diameter of hard phase increases gradually and reaches about 110 μm at a temperature of 110 °C and a strain rate of 2500 s^{-1}.

3.2 The Original Johnson–Cook Model

The original Johnson–Cook model is frequently used to consider the strain rate and temperature effects on the constitutive relation due to its wide range of applicability and its simple form. The constitutive equation of this model is given as follows:

$$\sigma = (A + B\varepsilon^n)(1 + C_1 \ln \dot{\varepsilon}^*)(1 - T^{*m}) \qquad \text{(Eq 1)}$$

where σ is the von Mises equivalent flow stress, ε is the equivalent plastic strain. $\dot{\varepsilon}^*$ is the dimensionless strain rate, which is obtained from $\dot{\varepsilon}^* = \dot{\varepsilon}/\dot{\varepsilon}_{\text{ref}}$, where $\dot{\varepsilon}$ is the strain rate and $\dot{\varepsilon}_{\text{ref}}$ is the reference strain rate, with 0.001 s^{-1}, and T^* is the relative temperature, which is obtained from $T^* = (T - T_{\text{ref}})/(T_m - T_{\text{ref}})$, where T is the experimental temperature, T_{ref} is the reference temperature and T_m is the melting temperature. In this work, the values of T_{ref} and T_m are 20 °C and 300 °C, respectively. The meanings of the constants are as follows: A is
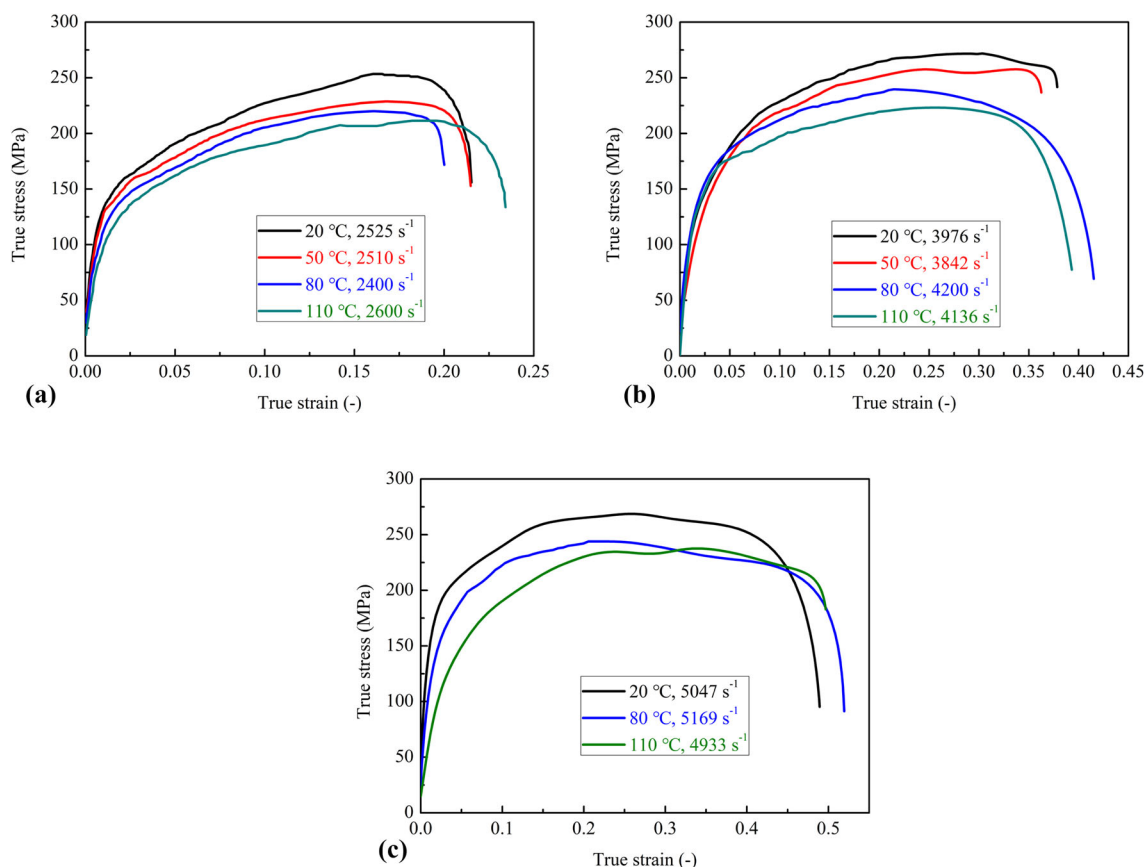

Fig. 5 Experimental results of the true stress–strain curves at different temperatures at preset strain rates of (a) 2500 s^{-1}, (b) 4000 s^{-1}, (c) 5000 s^{-1}
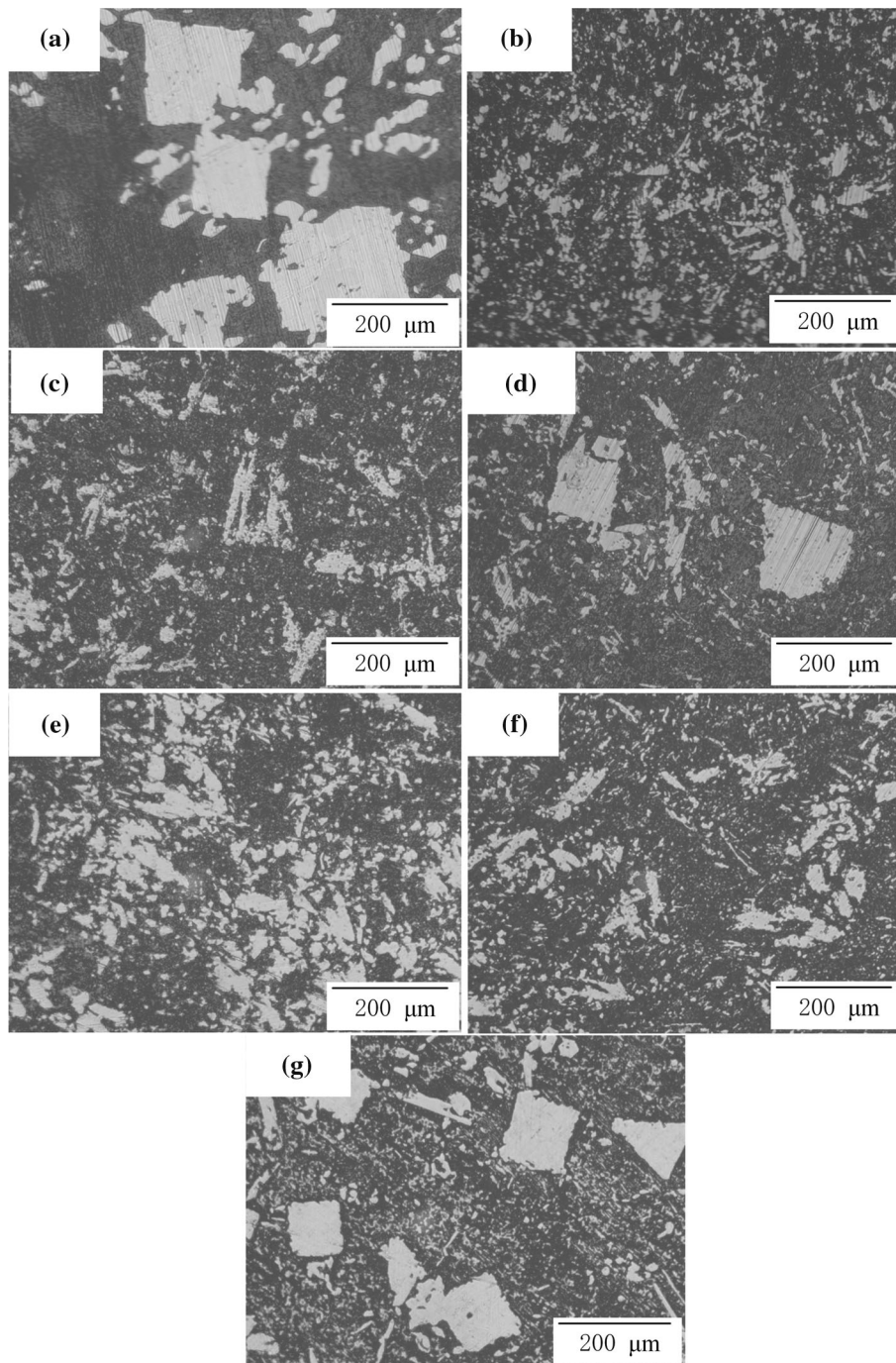
Fig. 6 SEM of the SnSbCu alloy at different loading conditions: (a) undeformed, (b) 20 °C and 2500 s^{-1}, (c) 20 °C and 4000 s^{-1}, (d) 20 °C and 5000 s^{-1}, (e) 50 °C and 2500 s^{-1}, (f) 80 °C and 2500 s^{-1}, (g) 110 °C and 2500 s^{-1}

the yield stress at the reference strain rate and reference temperature B is the material hardening coefficient, n is the material strain hardening index, C_1 is the strain rate sensitivity coefficient, and m is the temperature softening index. Note that $(A + B\varepsilon^n)$, $(1 + C_1 \ln \dot{\varepsilon}^*)$ and $(1 - T^{*m})$ represent the strain hardening effect, strain rate effect and temperature softening effect of the material, respectively. The effects of the three factors on the flow stress are not coupled; thus, the coefficients in each term of the original Johnson–Cook constitutive equation can be obtained separately by using the method described hereafter.

3.2.1 Determination of Constants A, B and n. Figure 7 shows the engineering stress–strain results of the quasi-static compressive experiment at the reference strain (0.001 s^{-1}) and the reference temperature (20 °C). Under this condition, Eq. (1) can be reduced as follows:

$$\sigma = (A + B\varepsilon^n) \qquad (Eq\ 2)$$

In addition, Eq. (2) can be converted into the following form,

$$\ln(\sigma - A) = n \ln \varepsilon + \ln B \qquad (Eq\ 3)$$

As previously mentioned, the constant A represents the yield stress, which could be obtained directly from the quasi-static test results shown in Fig. 8. The values of B and n could be acquired from the fitting line of the relation between $\ln(\sigma - A)$ and $\ln\varepsilon$. The constant n is the slope of the fitted line, and $\ln B$ is the intercept.

3.2.2 Determination of Constant C_1. When the temperature is 20 °C (i.e., the reference temperature), the softening term $(1 - T^{*m})$ in Eq. (1) is eliminated since T^* is zero, and then, Eq. (1) can be reduced as follows:

$$\sigma = (A + B\varepsilon^n)(1 + C_1 \ln \dot{\varepsilon}^*) \qquad (Eq~4)$$

Equation (4) can be transformed into the following form

$$\frac{\sigma}{A + B\varepsilon^n} = 1 + C_1 \ln \dot{\varepsilon}^* \qquad (Eq~5)$$

As previously described, the constants A, B and n were already obtained; hence, the value of C_1 could be acquired from the relation between $\sigma/(A + B\varepsilon^n)$ and $\ln\dot{\varepsilon}^*$. Several sets of stress and strain should be selected to fit the line.
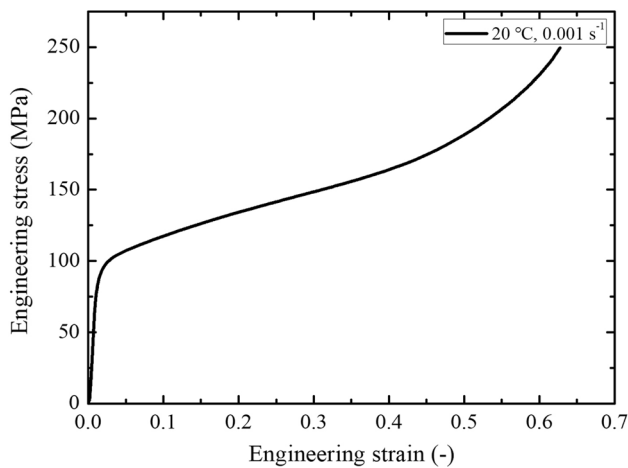

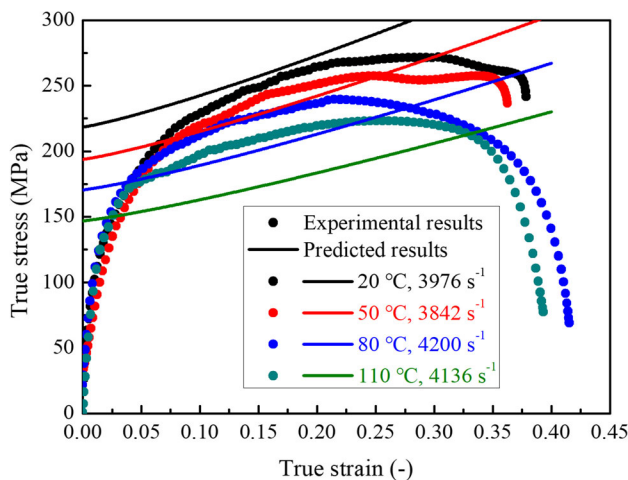**Fig. 7** Quasi-static compressive stress–strain curve

Fig. 8 Comparison between the experimental data and the predicted values by the original Johnson–Cook model

3.2.3 Determination of Constant m. When the strain rate equals the reference strain rate 0.001 s^{-1}, the term of $(1 + C_1 \ln \dot{\varepsilon}^*)$ was eliminated since $\dot{\varepsilon}^* = 1$; thus, Eq. (1) can be reduced to the following form:

$$\sigma = (A + B\varepsilon^n)(1 - T^{*m}) \qquad (Eq~6)$$

The value of m could be derived as the slope of the fitting line by fitting the relationship between $\ln(1 - \sigma/(A + B\varepsilon^n))$ and $\ln T^*$.

Therefore, the constants of the Johnson–Cook model for the SnSbCu alloy are acquired and listed in Table 2, and the corresponding constitutive equation is given as shown in Eq. (7):

$$\sigma = (102 + 171.3\varepsilon^{1.185})(1 + 0.0752 \ln \dot{\varepsilon}^*)(1 - T^{*0.98}) \qquad (Eq~7)$$

To check the accuracy of the selected constitutive relation, the predicted results given by Eq. (7) and the experimental results at a chosen strain rate of 4000 s^{-1} are compared as shown in Fig. 8. For low temperatures, the deviation between the predicted results and the experimental results is small in the plastic stage; whereas the temperature increases, the deviation increases. To further verify the accuracy of the model, the correlation coefficient (R) and the absolute average relative error (AARE) were used to evaluate the predictive capability of the model (Ref 36, 37). R represents the intensity of the linear relation between the predicted and experimental data, and AARE represents the actual situation of the error between the data. These coefficients can be expressed as follows:

$$R = \frac{\sum_{i=1}^{i=N} \left(\sigma_e^i - \bar{\sigma}_e\right)\left(\sigma_p^i - \bar{\sigma}_p\right)}{\sqrt{\sum_{i=1}^{i=N} \left(\sigma_e^i - \bar{\sigma}_e\right)^2 \sum_{i=1}^{i=N} \left(\sigma_p^i - \bar{\sigma}_p\right)^2}} \qquad (Eq~8)$$

$$\text{AARE}(\%) = \frac{1}{N}\sum_{i=1}^{i=N} \left|\frac{\sigma_e^i - \sigma_p^i}{\sigma_e^i}\right| \times 100 \qquad (Eq~9)$$

where σ_e^i is the experimental plastic stress data, σ_p^i is the predicted plastic stress obtained from the model; $\bar{\sigma}_e$ and $\bar{\sigma}_P$ represent the average of σ_e^i and σ_p^i, respectively; and N is the number of data points selected at the plastic process.

At a temperature of 20 °C, R is larger than 0.92 and AARE is 6.7%, which shows that accuracy of the model is acceptable. As the temperature increased, the value of R decreased to 0.8380, and the value of AARE increased to 15%, indicating that the predicted results are not sufficiently reliable. This phenomenon mainly occurs because the original J–C model assumes that the strain rate effect is independent of the temperature effect. However, many materials would produce new effects at high temperatures and high strain rates. It cannot simply be assumed that the effects of flow stress from temperature, strain and strain rate have no interaction. Therefore, it is difficult to state that the original J–C model can

Table 2 Constants of the original J–C model for the SnSbCu alloy

Constant	A, MPa	B, MPa	n	C_1	m
Value	102	171.3	1.185	0.0752	0.98

describe the constitutive relation of the SnSbCu alloy with sufficient accuracy within the temperature range from 20 °C to 110 °C.

3.3 Modified Johnson–Cook model

As mentioned before, the original J–C model could not exactly describe the flow behaviors of the SnSbCu alloy material within the temperature of 20-110 °C. Therefore, this original J–C model should be modified. Many current modified J–C models (Ref 38, 39) considered different coupling effects among strain, strain rate and temperature to overcome the limitations in the original J–C model. For example, Wang et al. (Ref 27) modified the original J–C model by replacing the constant C_1 with a function related to the strain rate and temperature, and the predicted values obtained by their modified model were closer to the experimental results than the original J–C model. Tan et al. (Ref 40) also considered the coupled effect of the strain and strain rate on the constant C_1 to modify the original J–C model and obtained more accurate prediction results. Thus, in this work, the coupled effect of the strain rate and temperature on the C_1 value was considered to modify the original J–C model. Moreover, the expression of the strain effect was also improved to further increase the accuracy of the prediction.

The complete description of the modified Johnson–Cook model is:

$$\sigma = \left(A_1 + B_1\varepsilon + B_2\varepsilon^2 + B_3\varepsilon^3\right)\left(1 + C_1 \ln \dot{\varepsilon}^*\right)\left(1 - T^{*m}\right) \quad (\text{Eq } 10)$$

where A_1, B_1, B_2 and B_3 are the newly introduced material constants and m is the same as that used in the original J–C model. The function $C_1 = f\left(\dot{\varepsilon}, T\right)$ was used to describe the effect of the strain rate and temperature on the value of C_1.

3.3.1 Determination of Constants A_1, B_1, B_2 and B_3. When the strain rate was 0.001 s^{-1} and the temperature was 20 °C, the terms of $\left(1 + C_1 \ln \dot{\varepsilon}^*\right)$ and $\left(1 - T^{*m}\right)$ were eliminated since $\dot{\varepsilon}^* = 1$ and $T^* = 1$; thus, Eq. (10) is transformed to the following form:

$$\sigma = A_1 + B_1\varepsilon + B_2\varepsilon^2 + B_3\varepsilon^3 \quad (\text{Eq } 11)$$

After substituting the experimental data at the reference strain rate and temperature into Eq. (11), the stress–strain curve (shown in Fig. 9) is drawn and subjected to cubic polynomial fitting to obtain A_1, B_1, B_2 and B_3.

3.3.2 Determination of Constant m. When the strain rate equals the reference strain rate 0.001 s^{-1}, Eq. (10) is transformed to the following form:

$$\sigma = \left(A + B_1\varepsilon + B_2\varepsilon^2 + B_3\varepsilon^3\right)\left(1 - T^{*m}\right) \quad (\text{Eq } 12)$$

Similarly, Eq. (12) can be expressed as follows:

$$\ln\left(1 - \frac{\sigma}{A + B_1\varepsilon + B_2\varepsilon^2 + B_3\varepsilon^3}\right) = m \ln T^* \quad (\text{Eq } 13)$$

The stress at seven different values of strain (0.1, 0.15, 0.2, 0.25, 0.3, 0.35, 0.4) and three different temperatures (50 °C, 80 °C, 110 °C) under the same strain rate is chosen to fit the relation between $\ln(1 - \sigma/(A_1 + B_1\varepsilon + B_2\varepsilon^2 + B_3\varepsilon^3))$ and $\ln T^*$,
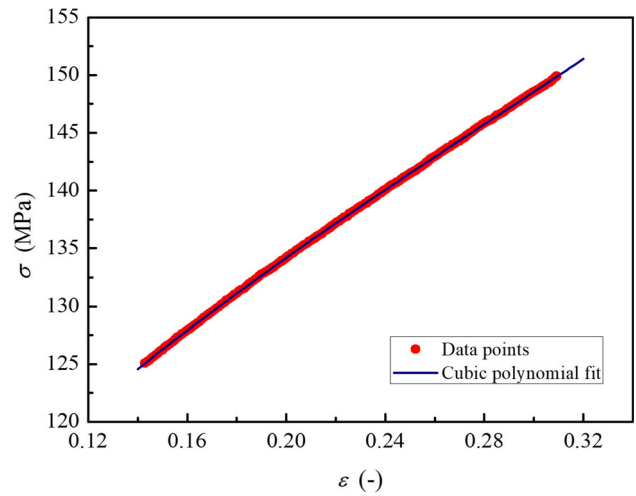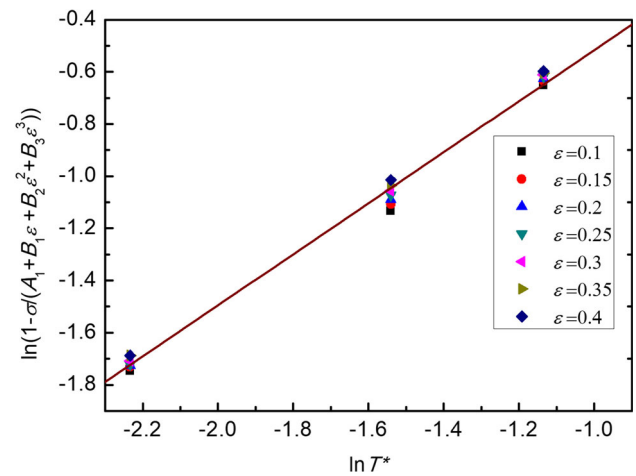
Fig. 9 Curve of fit and experimental data

Fig. 10 Relation between $\ln(1 - \sigma/(A_1 + B_1\varepsilon + B_2\varepsilon^2 + B_3\varepsilon^3))$ and $\ln T^*$

Table 3 The values of C_1 at different strain rates and temperature

Preset strain rate, s^{-1}	Temperature, °C			
	20	50	80	110
1000	0.04952	0.06587	0.08816	0.11340
2500	0.05454	0.06550	0.07445	0.09795
4000	0.04905	0.05527	0.08613	0.09820
5000	0.04414	0.05838	0.09266	0.09766

as shown in Fig. 10. Thus, the value of m could be obtained through the fitting line.

3.3.3 Determination of C_1. When the strain rate factor C_1 is solved, it can be found that the values change notably according to the strain rate and temperature, as shown in
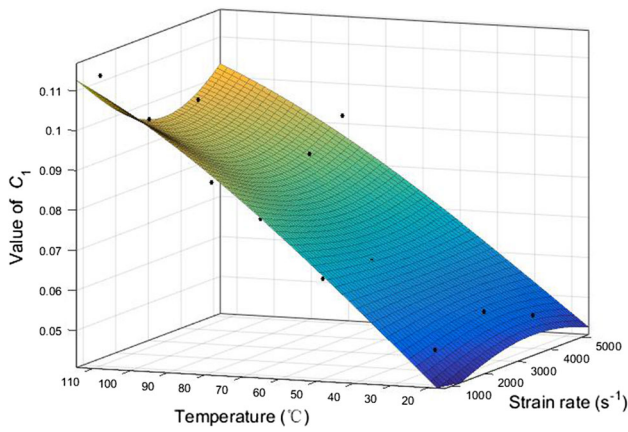
Fig. 11 Fitting results of the value of C_1 versus strain rate and temperature

Table 3. Therefore, the C_1 values at the different strain rates and temperature in Table 3 were fitted using the method of separation of variables by Warnecke and Oh (Ref 41), which can be expressed by the following equation:

$$C_1 = a - \left[b + d \sin\left(\frac{\dot{\varepsilon} - 1000}{5000}\pi\right)\right]\left[\sin\left(\frac{T - 20}{300}\pi\right)\right]$$

(Eq 14)

The fitting result is shown in Fig. 11, and the data points from the experimental results are close to the fitting surface.

Finally, the material constants of the modified J–C constitutive model for the SnSbCu alloy are given in Table 4. The relation between the stress and the strain for the different strain rates and temperatures is obtained according to the modified Johnson–Cook model:

Table 4 Constants of the modified J–C model for the SnSbCu alloy

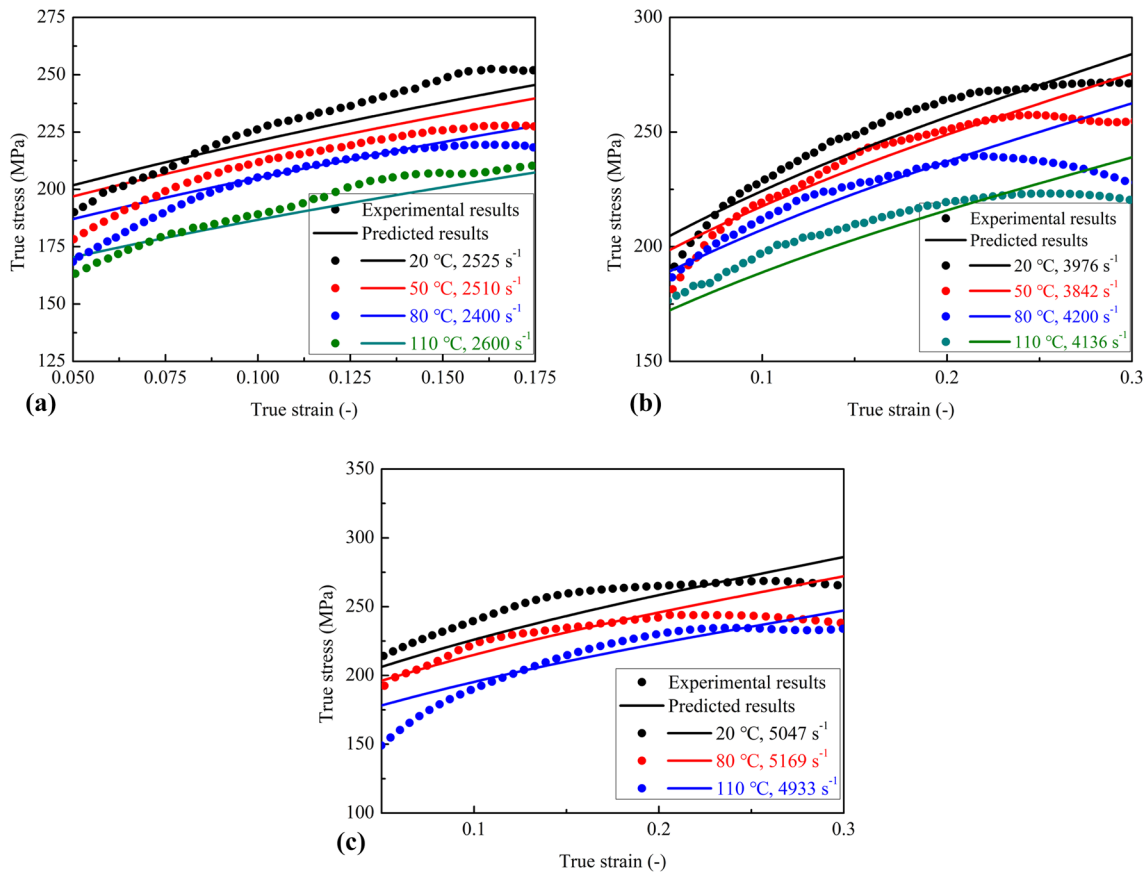| Constant	A_1, MPa	B_1, MPa	B_2, MPa	B_3, MPa	a	b	d	m
Value	95.05	206.2	− 421.9	496.8	0.06	− 0.05554	0.01777	0.98

Fig. 12 Comparison between the experimental data and predicted values by the modified J–C model at preset strain rates of: (a) 2500 s^{-1}, (b) 4000 s^{-1} and (c) 5000 s^{-1}

$$\sigma = \left(95.05 + 260.2\varepsilon - 421.9\varepsilon^2 + 496.8\varepsilon^3\right)$$
$$\left(1 - \frac{(T-20)^{0.98}}{(300-20)}\right)$$
$$\left\{1 + \left[0.06 - \left(-0.05554 + 0.01777\sin\left(\frac{\dot{\varepsilon} - 1000}{5000}\pi\right)\right)\right.\right.$$
$$\left.\left.\sin\left(\frac{T-20}{300}\pi\right)\right]\ln\frac{\dot{\varepsilon}}{0.001}\right\}$$

(Eq 15)

3.4 Analysis of the Modified J–C Model Accuracy

Several sets of representative experimental stress–strain data were chosen for comparison with those predicted by the modified J–C model at high strain rates (2500 s^{-1}, 4000 s^{-1} and 5000 s^{-1}), as shown in Fig. 12. Unlike the original J–C model, which could accurately predict the compressive behaviors only at low temperatures, the modified J–C model could predict the stress–strain relation for a larger range of temperatures and strain rates with high precision. The values of R and AARE of the original J–C model and modified J–C model are obtained through a comparison with the experimental results as shown in Table 5. For the different strain rates and temperatures, the R value of the original J–C model ranges from 0.8099 to 0.9802 with an average value of 0.9129, and the AARE value ranges from 3.6% to 15% with an average value of 9.2%. In comparison, the range of R values is from 0.8807 to 0.9930 wherein the average value is 0.9475, and the range of AARE values is from 2.5% to 4.9%, wherein the average value is 3.8%. The above data indicate that the predicted values obtained from the modified J–C constitutive model are closer to the experimental values than those predicted by the original J–C model; therefore, it could conclude that the modified J–C constitutive model can predict the compressive flow behaviors of SnSbCu alloy more accurately at high strain rates and temperatures. Moreover, this result also indicates that for the SnSbCu alloy material, the coupled effect of the temperature and the strain rate should be considered when the stress–strain relation is revealed.

3.5 LS-DYNA Simulation Verification

Furthermore, finite element analysis was used to verify the modified J–C constitutive model. The dynamic compression

Table 5 Values of R and $AARE$ of the original J–C model and modified J–C model obtained through a comparison with the experimental results

Strain rate, s^{-1}	Temperature, °C	Original J–C model		Modified J–C model	
		R	AARE, %	R	AARE, %
2525	20	0.9802	11	0.9930	4.5
2510	50	0.9598	6.5	0.9797	6.2
2400	80	0.9686	7.2	0.9820	4.9
2600	110	0.9675	12	0.9846	3.6
3976	20	0.9251	6.7	0.9587	2.5
3842	50	0.8980	3.6	0.9377	2.5
4200	80	0.8380	8.3	0.8884	3.1
4136	110	0.9193	15	0.9535	3.1
5047	20	0.8646	5.2	0.9210	4.3
5169	80	0.8099	10	0.8807	3.7
4933	110	0.8994	15	0.9428	3.6
Average		0.9129	9.2	0.9475	3.8

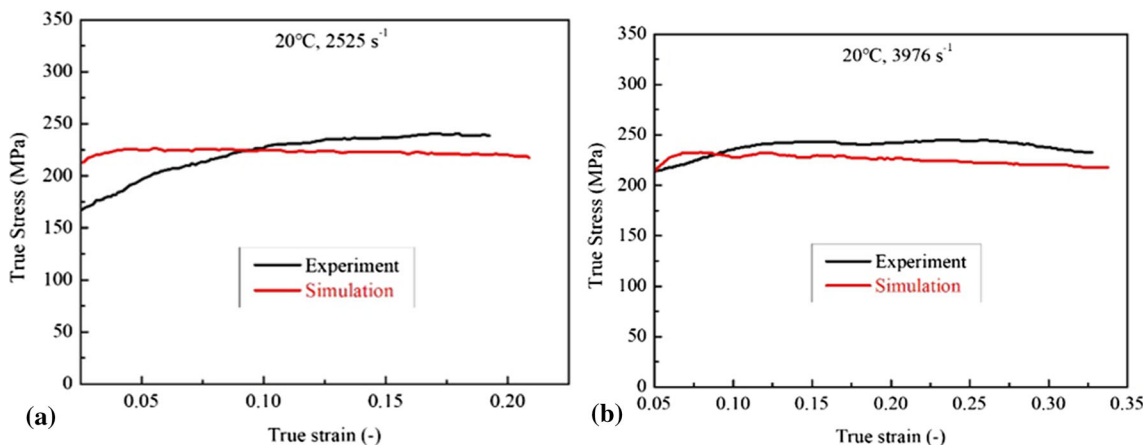**Fig. 13** Comparison of the true stress–strain curves form the experiment and simulation at: (a) 20 °C and 2525 s^{-1} and (b) 20 °C and 3976 s^{-1}

process of the SnSbCu alloy was simulated using LS-DYNA (Ref 42). A model is developed according to the above-mentioned SHPB experimental conditions, where the diameters of the bullet, the incident bar and the transmitted bar are all 16 mm, the bullet length is 20 cm and the lengths of the incident bar and the transmitted bar are both 100 cm. SOLID164 elements were used to model the geometries. Mapped face meshing was selected, and the finite element model was divided into 36 girds per 5 mm. The unconstrained boundary condition was adopted, and the solution method was set as the explicit dynamic solution.

The modified J–C constitutive model, which was previously obtained, was substituted into the finite element model, and the dynamic compression process of the alloy was calculated. The data of the incident bar and the transmitted bar were extracted to calculate the stress–strain curve. Figure 13 shows a comparison of experimental data and simulation data for strain rates of 2525 s^{-1} and 3976 s^{-1} at a temperature of 20 °C. The stress–strain curve obtained by the finite element simulation agrees with the curve obtained by the experimental tests. This comparison could further verify the accuracy of the modified J–C constitutive model at high strain rates and temperatures.

4. Conclusion

In this work, the compressive flow behaviors of the SnSbCu alloy were investigated at strain rates of 1000-5000 s^{-1} and at temperatures of 20-110 °C. Several conclusions can be drawn from this work, as described hereafter:

(1) For the SnSbCu alloy, the strain rate hardening effect was influenced by the temperature, i.e., these two factors are not independent as assumed in the original Johnson–Cook constitutive model. Thus, the original J–C model could not accurately describe the compressive flow behaviors at high temperatures and high strain rates.

(2) A modified Johnson–Cook model was developed by considering the value of C_1 as a function of the strain rate and temperature, to consider the coupled effect of strain rate and temperature on the constitutive relation of the SnSbCu alloy. According to the accuracy analysis and the finite element dynamic analysis, the modified J–C model shows good applicability in the focused temperature range and at high strain rates, which means that the modified J–C model could be used to predict the compressive behaviors of SnSbCu alloy at the high strain rates and high temperature selected in this work.

Acknowledgments

References

1. L. Gambirasio and E. Rizzi, An Enhanced Johnson–Cook Strength Model for Splitting Strain Rate and Temperature Effects on Lower Yield Stress and Plastic Flow, *Comput. Mater. Sci.*, 2016, **113**, p 231–265

2. R. Bobbili, and V. Madhu. A Modified Johnson–Cook Model for FeCoNiCr High Entropy Alloy Over a Wide Range of Strain Rates. *Mater. Lett.*, 2018: S0167577X18301812

3. W.D. Song, J.G. Ning, X.N. Mao, and H.P. Tang, A Modified Johnson–Cook Model for Titanium Matrix Composites Reinforced with Titanium Carbide Particles at Elevated Temperatures, *Mater. Sci. Eng. A Struct. Mater. Prop. Microstruct. Process.*, 2013, **576**, p 280–289

4. D.N. Zhang, Q.Q. Shangguan, C.J. Xie, and F. Liu, A Modified Johnson–Cook Model of Dynamic Tensile Behaviors for 7075-T6 Aluminum Alloy, *J. Alloys Compd.*, 2015, **619**, p 186–194

5. G.J. Chen, L. Chen, G.Q. Zhao, C.S. Zhang, and W.C. Cui, Microstructure Analysis of an Al-Zn-Mg Alloy During Porthole Die Extrusion Based on Modeling of Constitutive Equation and Dynamic Recrystallization, *J. Alloys Compd.*, 2017, **710**, p 80–91

6. G.R. Johnson, and W.H. Cook. A Constitutive Model and Data for Metals Subjected to Large Strains, High Strain Rates, and High Temperatures. In: Proceedings of the Seventh International Symposium on Ballistics, International Ballistics Committee, The Hague, Netherlands, 1983, p 541–7

7. D.J. Bammann, M.L. Chiesa, and G.C. Johnson, Modeling Large Deformation and Failure in Manufacturing Processes, *Theor. Appl. Mech.*, 1996, **9**, p 359–376

8. P.S. Follansbee and U.F. Kocks, A Constitutive Description of the Deformation of Copper Based on the Use of the Mechanical Threshold Stress as an Internal State Variable, *Acta Metall.*, 1988, **36**, p 81–93

9. F.J. Zerilli and R.W. Armstrong, Dislocation-Mechanics-Based Constitutive Relations for Material Dynamics Calculations, *J. Appl. Phys.*, 1987, **61**, p 1816–1825

10. S.N. Nasser and Y.L. Li, Flow Stress of fcc Polycrystals with Application to OFHC Cu, *Acta Mater.*, 1998, **46**, p 565–577

11. H.R.R. Ashtiani, M.H. Parsa, and H. Bisadi, Constitutive Equations for Elevated Temperature Flow Behavior of Commercial Purity Aluminum, *Mater. Sci. Eng. A*, 2012, **545**, p 61–67

12. G.F. Xu, X.Y. Peng, X.P. Liang, X. Li, and Z.M. Yin. Constitutive Relationship for High Temperature Deformation of Al-3Cu-0.5Sc Alloy. Trans. Nonferrous Met. Soc. China, 2013, 23: 1549–55

13. G.Z. Quan, Y. Shi, C.T. Yu, and J. Zhou, The Improved Arrhenius Model with Variable Parameters of Flow Behavior Characterizing for the as-Cast AZ80 Magnesium Alloy, *Mater. Res.*, 2013, **16**, p 785–791

14. D.N. Zou, K. Wu, Y. Han, W. Zhang, B. Cheng, and G.J. Qiao, Deformation Characteristic and Prediction of Flow Stress for as-Cast 21Cr Economical Duplex Stainless Steel Under Hot Compression, *Mater. Des.*, 2013, **51**, p 975–982

15. G.T. Gray, S.R. Chen, and K.S. Vecchio, Influence of Grain Size on the Constitutive Response and Substructure Evolution of MONEL 400, *Metall. Mater. Trans. A*, 1999, **30**, p 1235–1247

16. S.T. Chiou, W.C. Cheng, and W.S. Lee, Strain Rate Effects on the Mechanical Properties of a Fe-Mn-Al Alloy Under Dynamic Impact Deformations, *Mater. Sci. Eng., A*, 2005, **392**, p 156–162

17. J. Choung, W. Nam, and J.Y. Lee, Dynamic Hardening Behaviors of Various Marine Structural Steels Considering Dependencies on Strain Rate and Temperature, *Marine Struct.*, 2013, **32**, p 49–67

18. G.R. Johnson and W.H. Cook, Fracture Characteristics Of Three Metals Subjected to Various Strains, Strain Rates, Temperatures and Pressures, *Eng. Fract. Mech.*, 1985, **21**, p 31–48

19. Y. Prawoto, M. Fanone, S. Shahedi, M.S. Ismail, and W.B. Wan Nik, Computational Approach Using Johnson-Cook Model on Dual Phase Steel, *Comput. Mater. Sci.*, 2012, **54**, p 48–55

20. K. Vedantam, D. Bajaj, N.S. Brar, and S. Hill, Johnson–Cook Strength Models for Mild and DP 590 Steels//AIP Conference Proceedings, *AIP*, 2006, **845**, p 775–778

21. L. Chen, G.Q. Zhao, and J.Q. Yu, Hot Deformation Behavior and Constitutive Modeling of Homogenized 6026 Aluminum Alloy, *Mater. Des.*, 2015, **74**, p 25–35

22. A. Shrot and M. Bäker, Determination of Johnson–Cook Parameters from Machining Simulations, *Comput. Mater. Sci.*, 2012, **52**, p 298–304

23. X.G. Deng, S.X. Hui, W.J. Ye, and X.Y. Song, Construction of Johnson–Cook Model for Gr2 Titanium Through Adiabatic Heating Calculation, *Appl. Mech. Mater.*, 2014, **487**, p 7–14

24. D. Samantaray, S. Mandal, and A.K. Bhaduri, A Comparative Study on Johnson Cook, Modified Zerilli-Armstrong and Arrhenius-Type Constitutive Models to Predict Elevated Temperature Flow Behaviour in Modified 9Cr–1Mo Steel, *Comput. Mater. Sci.*, 2009, **47**, p 568–576

25. A. He, G.L. Xie, H.L. Zhang, and X.T. Wang. A Comparative Study on Johnson–Cook, Modified Johnson–Cook and Arrhenius-Type Constitutive Models to Predict the High Temperature Flow Stress in 20CrMo Alloy Steel. Mater. Des. (1980–2015), 2013, 52: 677–85

26. H.Y. Li, X.F. Wang, J.Y. Duan, and J.J. Liu, A Modified Johnson Cook Model for Elevated Temperature Flow Behavior of T24 Steel, *Mater. Sci. Eng. A*, 2013, **577**, p 138–146

27. X.Y. Wang, C.Z. Huang, B. Zou, H.L. Liu, H.T. Zhu, and J. Wang, Dynamic Behavior and a Modified Johnson-Cook Constitutive Model of Inconel 718 at High Strain Rate and Elevated Temperature, *Mater. Sci. Eng. A*, 2013, **580**, p 385–390

28. Y.C. Lin and X.M. Chen, A Combined Johnson-Cook and Zerilli-Armstrong Model for hot Compressed Typical High-Strength Alloy Steel, *Comput. Mater. Sci.*, 2010, **49**, p 628–633

29. S. Gangireddy and S.P. Mates, High Temperature Dynamic Response of a Ti-6Al-4V Alloy: A Modified Constitutive Model for gradual Phase Transformation, *J. Dyn. Behav. Mater.*, 2017, **3**, p 557–574

30. H.Y. Li, Y.H. Li, X.F. Wang, J.J. Liu, and Y. Wu, A Comparative Study on Modified Johnson Cook, Modified Zerilli-Armstrong and Arrhenius-Type Constitutive Models to Predict the Hot Deformation Behavior in 28CrMnMoV Steel, *Mater. Des.*, 2013, **49**, p 493–501

31. J. Cai, K.S. Wang, P. Zhai, F.G. Li, and J. Yang, A Modified Johnson–Cook Constitutive Equation to Predict Hot Deformation Behavior of Ti-6Al-4V Alloy, *J. Mater. Eng. Perform.*, 2015, **24**, p 32–44

32. A. Shokry, A Modified Johnson–Cook Model for Flow Behavior of Alloy 800H at Intermediate Strain Rates and High Temperatures, *J. Mater. Eng. Perform.*, 2017, **26**, p 5723–5730

33. L. Chen, G.Q. Zhao, J. Gong, X.X. Chen, and M.M. Chen, Hot Deformation Behaviors and Processing Maps of 2024 Aluminum Alloy in as-Cast and Homogenized States, *J. Mater. Eng. Perform.*, 2015, **24**, p 5002–5012

34. C.A. Ross and J.W. Tedesco, Split-Hopkinson Pressure-Bar Tests on Concrete and Mortar in Tension and Compression, *Mater. J.*, 1989, **86**, p 475–481

35. Z.G. Gao, X.M. Zhang, M.A. Chen, Y.S. Zhao, H.J. Li, and B. Liu, Effect of Temperature on Dynamic Yield Stress and Microstructure of 2519A Aluminum Alloy at High Strain Rate, *Rare Metal Mater. Eng.*, 2009, **35**, p 881–886

36. M.R. Rokni, A. Zarei-Hanzaki, A.A. Roostaei, and A. Abolhasani, Constitutive Base Analysis of a 7075 Aluminum Alloy During Hot Compression Testing, *Mater. Des.*, 2011, **32**, p 4955–4960

37. S. Srinivasulu and A. Jain, A Comparative Analysis of Training Methods for Artificial Neural Network Rainfall–Runoff Models, *Appl. Soft Comput.*, 2006, **6**, p 295–306

38. Y.H. Zhao, J. Sun, J.F. Li, Y.Q. Yan, and P. Wang, A Comparative Study on Johnson–Cook and Modified Johnson–Cook Constitutive Material Model to Predict the Dynamic Behavior Laser Additive Manufacturing FeCr Alloy, *J. Alloys Compd.*, 2017, **723**, p 179–187

39. M.J. Kim, H.J. Jeong, J.W. Park, S.T. Hong, and H.N. Han, Modified Johnson–Cook Model Incorporated with Electroplasticity for Uniaxial Tension Under a Pulsed Electric Current, *Met. Mater. Int.*, 2018, **24**, p 42–50

40. J.Q. Tan, M. Zhan, S. Liu, T. Huang, J. Guo, and H. Yang, A Modified Johnson–Cook Model for Tensile Flow Behaviors of 7050-T7451 Aluminum Alloy at High Strain Rates, *Mater. Sci. Eng., A*, 2015, **631**, p 214–219

41. G. Warnecke and J.D. Oh, A New Thermo-Viscoplastic Material Model for Finite-Element-Analysis of the Chip Formation Process, *CIRP Ann. Manuf. Technol.*, 2002, **51**, p 79–82

42. B. Gladman. LS-Dyna Keyword Users' Manual. Livermore Software Corporation California, 2007